J Membrane Biol (2008) 222:17–30
DOI 10.1007/s00232-008-9099-3

Epithelial Barrier Modulation by a Channel Forming Peptide

Suma Somasekharan · Robert Brandt · Takeo Iwamoto · John M. Tomich · Bruce D. Schultz

Received: 12 December 2007 / Accepted: 21 February 2008 / Published online: 18 April 2008

Abstract NC-1059 is a synthetic channel-forming peptide that provides for ion transport across, and transiently reduces the barrier integrity of, cultured epithelial monolayers derived from canine kidney (MDCK cells). Experiments were conducted to determine whether epithelial cells derived from other sources were similarly affected. Epithelial cells derived from human intestine (T-84), airway (Calu-3), porcine intestine (IPEC-J2) and reproductive duct (PVD9902) were grown on permeable supports. Basal short circuit current (I_{sc}) was <3 μA cm^{-2} for T-84, IPEC-J2 and PVD9902 cell monolayers and <8 μA cm^{-2} for Calu-3 cells. Apical NC-1059 exposure caused, in all cell types, an increase in I_{sc} to >15 μA cm^{-2}, indicative of net anion secretion or cation absorption, which was followed by an increase in transepithelial conductance (in mS cm^{-2}: T-84, 1.6 to 62; PVD9902, 0.2 to 51; IPEC-J2, 0.3 to 26; Calu-3, 2.3 to 13). These results are consistent with the peptide affecting transcellular ion movement, with a likely effect also on the paracellular route. NC-1059 exposure increased dextran permeation when compared to basal permeation, which documents an effect on the paracellular pathway. In order to evaluate membrane ion channels, experiments were conducted to study the dose dependence and stability of the NC-1059-induced membrane conductance in *Xenopus laevis* oocytes. NC-1059 induced a dose-dependent increase in oocyte membrane conductance that remained stable for greater than 2 h. The results demonstrate that NC-1059 increases transcellular conductance and paracellular permeation in a wide range of epithelia. These effects might be exploited to promote drug delivery across barrier epithelia.

Keywords Transepithelial conductance · Short circuit current · Dextran permeability · MDCK · PVD9902 · IPEC-J2 · Calu-3

S. Somasekharan
Yale School of Medicine Cellular and Molecular Physiology, New Haven, CT, USA
e-mail: suma.somasekharan@yale.edu

R. Brandt · T. Iwamoto · J. M. Tomich
Department of Biochemistry, Kansas State University, Manhattan, KS, USA

T. Iwamoto
e-mail: iwamoto@ksu.edu

J. M. Tomich
e-mail: jtomich@ksu.edu

B. D. Schultz (✉)
Department of Anatomy and Physiology, Kansas State University, 1600 Denison Avenue, Coles Hall 228, Manhattan, KS 66506, USA
e-mail: bschultz@vet.ksu.edu

Introduction

NK_4-M2GlyR (KKKKPARVGLGITTVLTMTTGSSGSRA) is a synthetic channel-forming peptide whose sequence is based on the second transmembrane segment (M2) of the glycine receptor (GlyR) α-subunit (Broughman et al. 2001; Tomich et al. 1998; Wallace et al. 1997). Lysine residues were added to the N terminus of M2GlyR to increase aqueous solubility. It was shown subsequently that sequential removal of C-terminal residues from NK_4-M2GlyR reduced aggregation of the peptide in solution, and peptides truncated up to five residues from the C terminus retained ion transport properties (Broughman et al. 2002b). Hence, a palindromic peptide consisting of the 11 N-terminal residues from M2GlyR followed by a central leucine and then an inverse sequence of the N-terminal segment was synthesized to maximize

channel-forming activity (Broughman et al. 2002b). Proline residues were replaced with alanines to improve the chemical synthesis, to arrive at the final sequence KKKKAARVGLGI TTVLVTTIGLGVRAA, which was named NC-1059.

Apical exposure of MDCK cell monolayers to NC-1059 caused a concentration-dependent increase in short circuit current (I_{sc}) (Broughman et al. 2004), a measure of net ion transport. Furthermore, the apparent dissociation constant, k_{app}, was reported to be 50 μM, which is fourfold lower than that of the originally designated NK_4-M2GlyR. In these studies, transepithelial electrical conductance (g_{te}) began to increase with I_{sc} and continued to increase even after I_{sc} reached peak value and began to decline. Exposure of MDCK cell monolayers to NC-1059 also increased permeation of 9.5-kDa fluorescein isothiocyanate (FITC)–conjugated dextran, suggesting that a paracellular route was opened by NC-1059 (Broughman et al. 2004). g_{te} returned to pretreatment values within 2 days after NC-1059 exposure, the shortest time point tested (Broughman et al. 2004). These observations were very encouraging as there is a tremendous impetus to identify molecules that may serve as "absorption enhancers" to augment delivery of hydrophilic and large uncharged therapeutics across epithelial barriers (Kondoh and Yagi 2007).

Tight junctions are multimolecular complexes between apical intercellular regions of epithelial cells that regulate paracellular permeability. Several techniques are being investigated to selectively and transiently reduce barrier function of epithelia or endothelia to allow the diffusion of therapeutic molecules to the interstitial space. Calcium chelators and surfactants disrupt barrier integrity but have unacceptable side effects, including changes in cell function and diminished cell adhesion (Thompson et al. 1994). Peptides corresponding to the first and second extracellular loops of occludin, a tight junction protein, increased paracellular permeability but required several hours to show significant effects (Chung et al. 2001; Lacaz-Vieira et al. 1999; Tavelin et al. 2003; Wong and Gumbiner 1997). More recently, a modified occludin peptide was shown to be effective at high concentrations (1 mM) in enhancing permeability across airway epithelia (Everett et al. 2006). The zonula occludens toxin of *Vibrio cholerae* (ZOT) provides a natural alternative to increase the permeability of small intestinal epithelia (Fasano and Uzzau 1997). ZOT has a rapid onset (<20 min) and is reversible. Yet, ZOT has drawbacks as a more generalized cotherapeutic agent in that it is a large peptide (399 amino acids) dependent on the presence of a membrane receptor that may not be present in all epithelia (Fasano et al. 1995).

NC-1059 has the potential to be developed into a cotherapeutic that can increase the bioavailability of various drugs. NC-1059 is a small peptide that can be readily synthesized. Additionally, we hypothesize that NC-1059 can modulate barrier function of epithelia derived from varied sources. The goal of the present study was to determine the effect of NC-1059 on epithelial cell lines derived from a variety of tissues. This study evaluates the differences in I_{sc} response, changes in g_{te} and paracellular permeation between different epithelia when exposed to various concentrations of NC-1059. Additionally, studies were conducted using *Xenopus laevis* oocytes to isolate and characterize the effects of NC-1059 on membrane conductance independent of effects on cell–cell interactions.

Methods

Peptide Synthesis

NC-1059 was synthesized by solid phase peptide synthesis using 9-fluorenylmethoxycarbonyl chemistries and purified as described previously (Broughman et al. 2002a).

Chemicals and Stock Solutions

1-Ethyl-2-benzimidazolinone (1-EBIO) was purchased from Acros (Fisher Scientific, Pittsburgh, PA). Unless specified otherwise, all other chemicals used were purchased from Sigma-Aldrich (St. Louis, MO). NC-1059 was prepared as a 5 mM stock in deionized water immediately before addition to the experimental chamber.

Cell Culture

T-84 cells were obtained from Dr. Daniel Devor (University of Pittsburgh, Pittsburgh, PA) and maintained in culture as described previously (Broughman et al. 2001, 2004). Cells were grown on 25 cm^2 flasks (Corning, Corning, NY) with a medium containing a 1:1 mixture of Dulbecco's modified Eagle medium (DMEM) and Nutrient F12 (GIBCO, Grand Island, NY), 5% heat-inactivated fetal bovine serum (FBS; Atlanta Biologicals, Atlanta, GA) and 1% penicillin and streptomycin (GIBCO). Approximately 5 x 10^5 cells were seeded onto 1.13 cm^2 permeable supports (Snapwell; Corning). The medium was refreshed every other day until used for experimentation, with the last medium change occurring 1 day prior to analysis. All other cell types were maintained using similar techniques, with some exceptions noted below.

IPEC-J2 cells were provided by Dr. Anthony Blikslager (North Carolina State University, Raleigh, NC) and grown in a medium containing a 1:1 mixture of DMEM and Nutrient F12, 5% heat-inactivated FBS, 1% insulin-transferrin-selenium and 1% penicillin and streptomycin.

PVD9902 (Carlin et al. 2006) cells were grown in a medium containing DMEM, 10% heat-inactivated FBS and 1% penicillin and streptomycin. The PVD9902, IPEC-J2

and T-84 cells were grown on permeable supports, typically for 14 days prior to experimental evaluation.

Calu-3 cells were grown with a medium containing a 1:1 mixture of DMEM and Nutrient F12, 15% heat-inactivated FBS, 2 mM glutamine and 1% penicillin and streptomycin. Cells were grown on permeable supports for 28–34 days. The apical medium was removed on the second day, and cells were cultured without medium on the apical surface thereafter until evaluation.

Electrical Measurements

I_{sc} and transepithelial electrical potential were measured using a modified Ussing chamber (model DCV9; Navicyte, San Diego, CA) as described previously (Broughman et al. 2001, 2004). Monolayers were bathed symmetrically with Ringer solution (in mM: 120 NaCl, 25 $NaHCO_3$, 3.3 KH_2PO_4, 0.8 K_2HPO_4, 1.2 $MgCl_2$ and 1.2 $CaCl_2$) that was prepared fresh daily, maintained at 37°C and bubbled with 5% CO_2/95% O_2 to maintain pH and to provide mixing. Monolayers were clamped to 0 mV using a voltage-clamp apparatus (model 558C-5; Department of Bioengineering, University of Iowa, Iowa City, IA). A 5-s bipolar pulse was applied every 100 s to allow for g_{te} assessment. Data acquisition was performed at 1 Hz with an Intel-based computer using Aqknowledge software (v. 3.2.6; BIOPAC Systems, Santa Barbara, CA) and MP100A-CE interface. The current measured in response to the voltage pulse was used to calculate g_{te} using Ohm's law, $g_{te} = \Delta I/\Delta V$.

Xenopus Oocyte Isolation

Oocytes were isolated as described previously (Broughman et al. 2004) from human chorionic gonadotropin–treated *X. laevis* (Xenopus One, Ann Arbor, MI) that were housed individually at 17°C. All procedures involving animals were conducted in compliance with American Physiological Society guidelines and approved by the university IACUC. The follicular layer of the oocytes was removed using collagenase and trypsin inhibitor in ND-96 that was nominally Ca^{2+}-free (in mM: 96 NaCl, 1 KCl, 1 $MgCl_2$, 5 HEPES, pH 7.5). Oocytes were washed subsequently with nominally Ca^{2+}-free ND-96 and incubated in a hypotonic solution (0.1 M K_2HPO_4 and 0.1% bovine serum albumin) for 1 h with gentle rolling at 15-min intervals. Oocytes were then maintained in modified Barth's solution (in mM: 88 NaCl, 1 KCl, 0.3 $Ca[NO_3]_2$, 0.41 $CaCl_2$, 0.82 $MgSO_4$, 2.4 $NaHCO_3$, 10 HEPES, pH 7.5) containing penicillin and streptomycin at 17°C until used.

Membrane Conductance Measurements

Oocyte membrane conductance was measured as described previously (Broughman et al. 2004) using a two-electrode voltage-clamp technique. Recordings were conducted in ND-96 (in mM: 96 NaCl, 1 KCl, 1 $MgCl_2$, 1.8 $CaCl_2$, 5 HEPES). Briefly, the oocytes were impaled with glass pipettes having an Ag/AgCl electrode filled with 1 M KCl. The electrodes were connected to a voltage-clamp amplifier (Gene Clamp 500B; Axon Instruments, Foster City, CA) and an analog to digital converter (DigiData 1200, Axon Instruments). The software used for data acquisition and analysis was pClamp 9.0 (Axon Instruments). Oocyte recordings were carried out using two voltage-clamp protocols. In the first repeating "diary" protocol, oocytes were sequentially held at -30 mV for 128 ms and then held at −90, −30, 0 and 30 mV for a duration of 1,000 ms each (total protocol duration = 4,128 s). The protocol was repeated throughout the recording to assess the stability of the membrane conductance for the entire duration of the experiment. The second "step" protocol was employed to determine with greater accuracy the slope conductance of the oocyte. The protocol included nine 2,048-ms sweeps consisting of an initial 548 ms at −30 mV, followed by 1,000 ms at the step potential and ending with 500 ms at −30 mV. The step potential ranged from −100 to +60 mV at 20-mV increments. A mean current from the middle 250 ms of each step potential was used to construct a current–voltage relationship (I–V plot). Data were fitted by a linear regression, and slope conductance was obtained from the fit.

The dose dependence of the NC-1059-induced changes in *X. laevis* oocyte conductance was determined by making bolus additions of NC-1059 to a flowing bath. Doses of increasing size ranging 1.25–20 nmoles of NC-1059 were added to the bath (~0.5 ml bath with 0.5 ml/min flow rate). Each addition was made after the current reached a plateau following the previous exposure and the slope conductance had been determined using the protocol described above. To determine if the NC-1059-induced conductance remained stable for a long duration, oocytes were exposed to 5 nmoles of NC-1059 and, once the membrane conductance reached a stable value, the step protocol was conducted to determine the slope conductance. The step protocol was repeated periodically thereafter, with the entire recording lasting 2 h.

Dextran Permeability Assay

Dextran permeation through the monolayer was measured as described previously (Broughman et al. 2004). Media were removed and the monolayers washed with warm phosphate-buffered saline (PBS). In untreated and NC-1059-exposed monolayers, Ringer solution was added to the basolateral (1 ml) and apical (200 µl) compartments in the Snapwell culture system. NC-1059 was added to the Ringer solution on the apical side of the monolayers to result in a final concentration of 200 µM NC-1059. Monolayers were also exposed symetrically to 5 mM EDTA in hypotonic Ringer

solution (diluted 1:1 with deionized H_2O). FITC-conjugated dextran (0.5 mg of 10, 20, 40 or 70 kDa) was added to the apical compartment of all treatments. After incubation at 37°C for 1 h, samples were taken from the basolateral compartment for determination of fluorescence intensity (Fluorskan Ascent FL; Labsystems, Helsinki, Finland). A series of dilutions of each size of dextran was prepared, and fluorescence was determined as a function of concentration. A linear regression was used to derive the slope and to calculate the amount of dextran that permeated the monolayer.

Data Analysis

All results are reported as mean ± SEM. All graphs and regression fits were completed using Sigmaplot (v 6.0; SPSS, Inc., Richmond, CA) or Excel (v 11.8; Microsoft, Redmond, WA). Student's *t*-test (Sigmaplot) and analysis of variance (Excel) were used for statistical analysis where required. Concentration dependence was determined using the maximal I_{sc} recorded following exposure to each concentration of NC-1059. Kinetic parameters for concentration dependence were determined by fitting the following modified Hill equation (equation 1) to each data set:

$$I_{sc} = I_{sc\,min} + \frac{\Delta I_{sc\,max} \times [NC-1059]^b}{(k_{app})^b + [NC-1059]^b} \quad (1)$$

In the above equation $I_{sc\ min}$ is the basal I_{sc} prior to peptide addition, $\Delta I_{sc\ max}$ is the greatest increase in I_{sc} observed during exposure to a given concentration of NC-1059, the apparent K_D (k_{app}) is the concentration required to achieve half maximal ΔI_{sc} and b is the Hill coefficient.

The time course for NC-1059-induced changes in g_{te} was determined by fitting a sigmoidal function (equation 2) to values of g_{te} that were calculated every 100 s throughout each experiment using the time of NC-1059 exposure as the starting point for data acquisition.

$$g_{te} = g_{te\,min} + \frac{\Delta g_{te\,max}}{1 + e^{-\left[\frac{t-t_0}{b}\right]}} \quad (2)$$

In equation 2, $g_{te\,min}$ is the baseline conductance and $\Delta g_{te\,max}$ is the peak change in conductance reached during the recording for each concentration; b is inversely proportional to the slope at half $\Delta g_{te\ max}$. The data used for the fit were restricted to ~300 s after the peak g_{te} was reached.

Results

NC-1059 Induces a Change in Electrical Parameters for all Epithelia Tested

Experiments were conducted to determine if the concentration-dependent changes observed in I_{sc} and g_{te} with MDCK cells exposed apically to NC-1059 can be generalized to epithelia derived from different tissues and species. Typical and summarized results for each cell type are presented in Figs. 1–4.

T-84 Cells Derived from Human Colon

NC-1059 caused a concentration-dependent increase in I_{sc} and g_{te} across T-84 cell monolayers. Figure 1a shows the recording from a typical experiment in which an epithelial cell monolayer was exposed apically to NC-1059 (60 μM). An initial I_{sc} of 2 μA cm^{-2} was measured. The monolayer was exposed to 1-EBIO (300 μM) prior to peptide exposure, as indicated by the solid bar. 1-EBIO activates Ca^{2+}-sensitive K^+ channels, IK and SK (Devor et al. 1996b), hyperpolarizing the cells and thus increasing the electrochemical driving force for anion secretion. 1-EBIO can also activate the cystic fibrosis transmembrane regulator (CFTR) anion channel (Devor et al. 1996a), although at concentrations higher than required to activate K^+ channels. The concentration of 1-EBIO was selected because it is reported to produce a maximal activation of K^+ channels and to be below the half-maximal concentration for CFTR activation. Exposure of T-84 cells to 1-EBIO resulted in a variable increase in I_{sc} that was consistent with SK or IK activation and transient activation of CFTR channels. Once the I_{sc} attained a constant value, the monolayer was exposed to NC-1059. Exposure to the peptide was associated with a characteristic rapid increase in I_{sc} within 4 min from 4 to 38 μA cm^{-2}. Subsequently, I_{sc} declined toward baseline but remained elevated at ~17 μA cm^{-2} for more than 30 min. The magnitude of the current change generated in response to the bipolar pulse applied across the monolayers (represented by the vertical deflections in the I_{sc} trace) was used to calculate g_{te}. Initially, g_{te} was 0.55 mS cm^{-2}, and it increased to 0.75 mS cm^{-2} with exposure to 1-EBIO. g_{te} further increased immediately upon NC-1059 exposure along with the I_{sc}, which is expected with the introduction of ion channels in the apical membrane. At peak I_{sc}, g_{te} was 2.5 mS cm^{-2}. However, g_{te} continued to increase even after peak I_{sc} was attained and during the decline in I_{sc}. By the end of the recording presented in Fig. 1a, g_{te} had increased to 21 mS cm^{-2}. The results for concentration-dependent effects of NC-1059 on I_{sc} are summarized from six experiments in Fig. 1b. Prior to NC-1059 exposure, I_{sc} was 6.5 ± 1.5 μA cm^{-2} and maximal I_{sc}, with 200 μM NC-1059, was 65.8 ± 5.2 μA cm^{-2} ($n = 6$). The solid line represents the best fit of equation 1 to the data set. Results of the fit are presented in Table 1. It is noteworthy that the fit employed a Hill coefficient that was greater than unity, which suggests a complex reaction scheme and could be indicative of the peptide's assembly into oligomeric conductive pores. The average change in

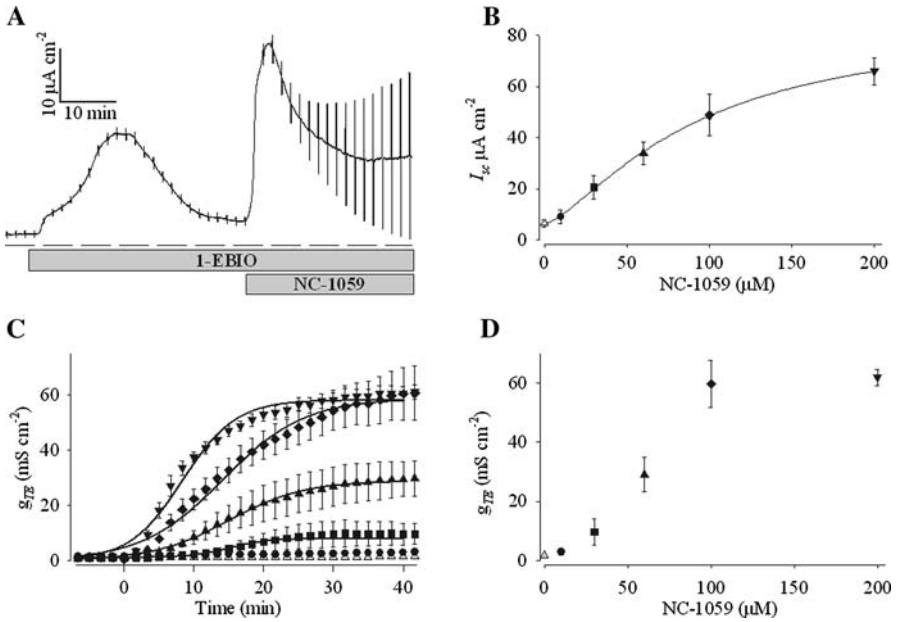

Fig. 1 NC-1059 induces a concentration-dependent elevation in I_{sc} and g_{te} across T-84 monolayers. (**A**) A representative trace of I_{sc} measured from a T-84 monolayer using a modified Ussing chamber. *Shaded bars* indicate the presence of 1-EBIO (300 μM) and apical exposure to NC-1059 (60 μM). (**B**) Maximal I_{sc} as a function of concentration. Symbols represent the maximal I_{sc} at the concentrations tested. *Solid line* represents a best fit of equation 1 to the data set, and parameters of the fit are presented in Table 1. (**C**) g_{te} vs. time for untreated (▲), 10 (•), 30 (■), 60 (▲), 100 (♦) and 200 (▼) μM NC-1059. *Solid lines* represent the best fit to equation 2 for the data set for 30, 60, 100 and 200 μM. (**D**) Maximum g_{te} as a function of concentration is plotted. (**B–D**) Data summarized from six observations for each concentration

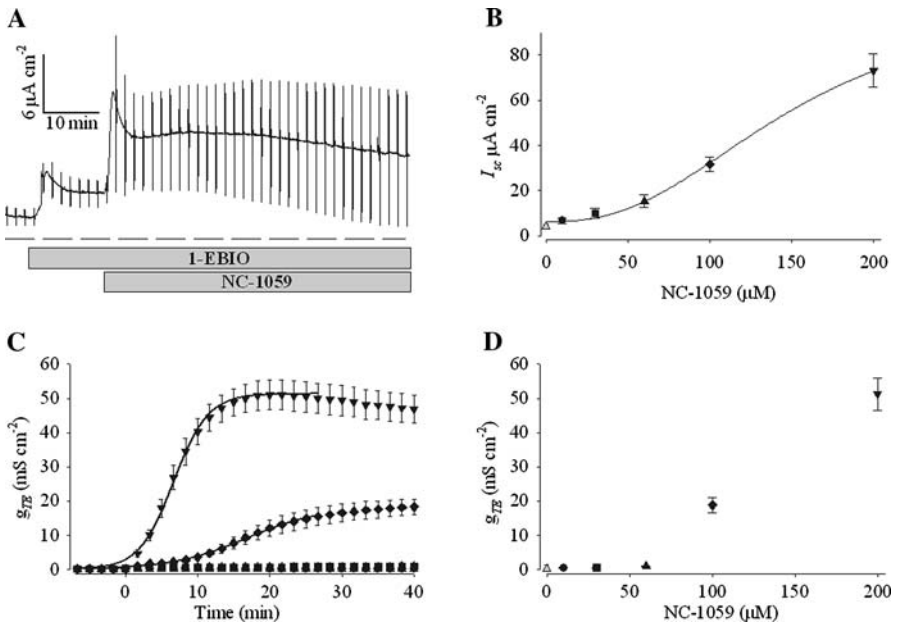

Fig. 2 NC-1059 induces a concentration-dependent elevation in I_{sc} and g_{te} across PVD9902 monolayers. (**A**) A representative trace of I_{sc} measured from a PVD9902 monolayer using a modified Ussing chamber. *Shaded bars* indicate the presence of 1-EBIO (300 μM) and apical exposure to NC-1059 (60 μM). (**B**) Maximal I_{sc} as a function of concentration. Symbols represent the maximal I_{sc} at the concentrations tested. *Solid line* represents the best fit of equation 1 to the data set. Parameters of the function are presented in Table 1. (**C**) g_{te} vs. time for untreated (▲), 10 (•), 30 (■), 60 (▲), 100 (♦) and 200 (▼) μM NC-1059. *Solid lines* represent the best fit to equation 2 for the data set of 100 and 200 μM. (**D**) Maximum g_{te} as a function of concentration is plotted. (**B–D**) Data summarized for six observations at each concentration

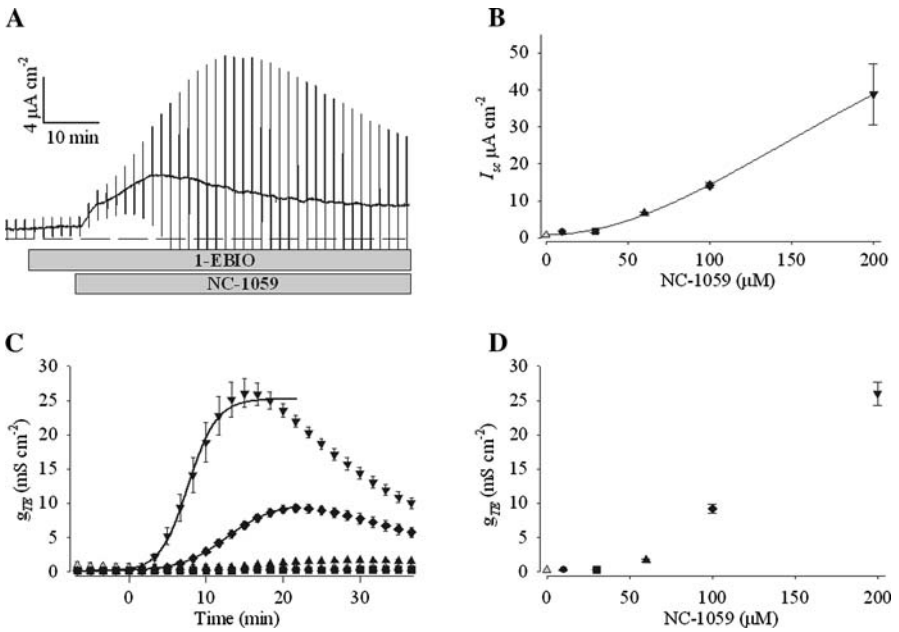

Fig. 3 NC-1059 induces a concentration-dependent change in I_{sc} and g_{te} across IPEC-J2 monolayers. (**A**) A representative trace of I_{sc} measured from IPEC-J2 monolayers using a modified Ussing chamber. *Shaded bars* indicate the presence of 1-EBIO (300 μM) and apical exposure to NC-1059 (60 μM). (**B**) Maximal I_{sc} as a function of concentration. Symbols represent the maximal I_{sc} at the concentrations tested. *Solid line* represents a best fit of equation 1 to the data set. Parameters of the function are presented in Table 1. (**C**) g_{te} vs. time for untreated (▲), 10 (•), 30 (■), 60 (▲), 100 (♦) and 200 (▼) μM NC-1059. *Solid lines* represent the best fit to equation 2 for the data set of 100 and 200 μM. (**D**) Maximum g_{te} as a function of concentration is plotted. (**B–D**) Data summarized for six observations at each concentration

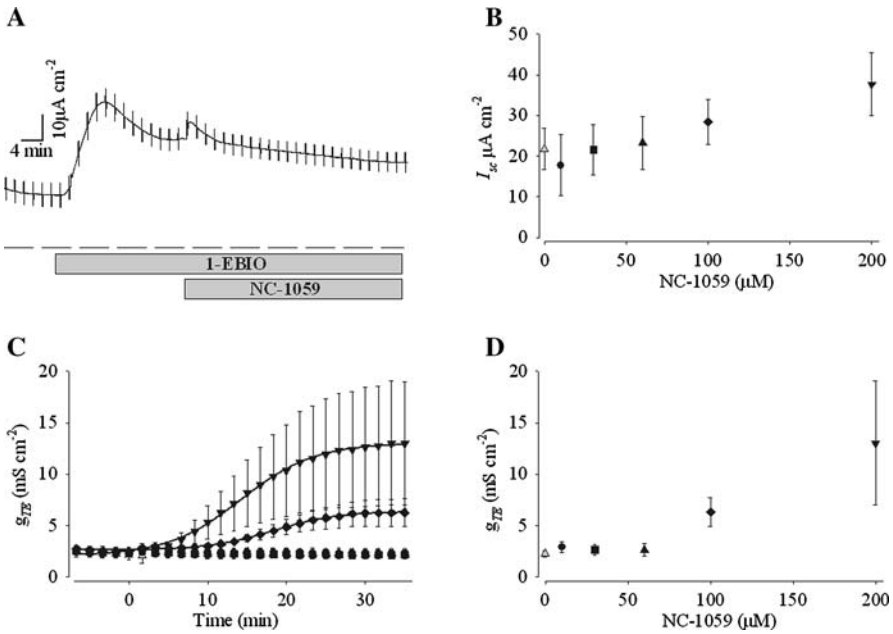

Fig. 4 NC-1059 induces a change in I_{sc} and g_{te} in Calu-3 monolayers. (**A**) A representative trace of I_{sc} measured from Calu-3 monolayers using a modified Ussing chamber. *Shaded bars* indicate the presence of 1-EBIO (300 μM) and apical exposure to NC-1059 (60 μM). (**B**) Maximal I_{sc} as a function of concentration. Symbols represent the maximal I_{sc} at the concentrations tested. (**C**) g_{te} vs. time for untreated (▲), 10 (•), 30 (■), 60 (▲), 100 (♦) and 200 (▼) μM NC-1059. *Solid lines* represent a best fit of equation 2 for the data set of 100 and 200 μM. (**D**) Maximum g_{te} as a function of concentration is plotted. (**B–D**) Data summarized from six experiments

g_{te} for each concentration as a function of time is provided in Fig. 1c. The graph revealed that the conductance increased with peptide exposure from a value of ~1 mS cm^{-2} to a maximal value in about 30 min and remained elevated throughout the experiment. A significant increase in g_{te} was observed with 30 μM, and maximal g_{te} increased with concentration, reaching a maximal value at 100 μM. The peptide at 200 μM did not elicit a response greater than that observed with 100 μM. Parameters derived when equation 2 was fitted to the data sets for 100 and 200 μM are reported in Table 2. The results indicate that the half-maximal response occurred more quickly with exposure to 200 μM than 100 μM, although the maximal conductances were nearly identical. The time to reach half-maximal g_{te}

Table 1 Baseline values and parameters derived from the fit of the modified Hill equation

Cell line	Initial values		Values in the presence of 1-EBIO		Parameters derived with equation 1		
	I_{sc} (μA)	g_{te} (mS)	I_{sc} (μA)	g_{te} (mS)	$\Delta I_{sc\ max}$ (μA)	k_{app} (μM)	Hill coefficient
T-84	2.3 ± 0.4	0.87 ± 0.24	6.6 ± 1.5	1.65 ± 0.67	79.1 ± 31.8	91.1 ± 54.8	1.4 ± 0.7
PVD9902	2.0 ± 0.3	0.17 ± 0.02	4.0 ± 1.1	0.23 ± 1.05	100 ± 52[a]	152 ± 73	2.5 ± 1.1
IPEC-J2	0.8 ± 0.1	0.14 ± 0.01	0.7 ± 0.4	0.29 ± 0.06	100 ± 324[a]	256 ± 743	2.0 ± 2.0
Calu-3	7.6 ± 2.5	2.33 ± 0.40	21.0 ± 5.0	2.26 ± 0.33			

[a] Values constrained during fitting

(t_0) was greatest with 30 μM NC-1059 (17.1 ± 0.1 min) and decreased with increasing concentration, suggesting a concentration-dependent effect on the lag time to reach half-maximal change in g_{te}. Additionally, the slope ($1/b$) was greater for 200 μM compared to 100 μM, further suggesting a concentration-dependent effect on the rate of change in g_{te}. The peak conductance as a function of concentration is provided in Fig. 1d. Little change in g_{te} was observed with 10 μM NC-1059 compared to untreated monolayers. The g_{te} was significantly greater following exposure to 30 μM NC-1059, and a maximal g_{te} value of ~58 mS cm^{-2} was observed with both 100 and 200 μM. The maximal g_{te} that is reported approached the limit that the system can detect reliably.

PVD9902 Cells Derived from Porcine Vas Deferens

Figure 2a shows a typical recording of a PVD9902 monolayer exposed to 60 μM NC-1059. Exposure to 300 μM 1-EBIO resulted in a small change in I_{sc} but little change in g_{te}. Subsequent exposure to 60 μM NC-1059 was associated with an increase in I_{sc} from 5 to 15 μA cm^{-2}. I_{sc} reached a peak in less than 2 min and declined to a lower, but still elevated, level. There was an increase in g_{te} from 0.17 to 1.2 mS cm^{-2}, and g_{te} remained elevated throughout the recording. Average maximal I_{sc} as a function of concentration is summarized from six experiments in Fig. 2b. In PVD9902 cell monolayers, the average I_{sc} prior to NC-1059 exposure, but after exposure to 1-EBIO, was 4.0 ± 0.4 μA cm^{-2} and a significant effect of the peptide on I_{sc} was observed at 60 μM, with greater responses at 100 and 200 μM. The change in I_{sc} did not show any indication of a plateau within this concentration range of NC-1059, and hence, the fit to equation 1 was constrained to a maximal I_{sc} of 100 μA cm^{-2}. The solid line represents the best fit of the data with equation 1 (see Table 1). Figure 2c provides the concentration-dependent changes in g_{te} as a function of time with PVD9902 monolayers exposed to various concentrations of NC-1059. On the scale shown, no observable change in g_{te} was seen with either 30 or 60 μM. A significant change in g_{te} was observed at 100 μM, and g_{te} was nearly threefold greater with 200 μM. The parameters derived from the fit of equation 2 (Table 2) showed that PVD9902 monolayers exposed to 200 μM NC-1059 reached half-maximal g_{te} more rapidly than at 100 μM, with a difference that was nearly 10 min. Also, the slope ($1/b$) derived from the fit was steeper for 200 μM than 100 μM. The g_{te} began to decline gradually, which limited the duration of the fit. The peak conductance as a function of concentration in PVD9902 is provided in Fig. 2d. Again, no significant differences in g_{te} were observed for concentrations ≤60 μM. As shown in Fig. 2c and d, substantial increases in g_{te} occurred following exposure to 100 μM NC-1059, with even greater effect at 200 μM.

IPEC-J2 Cells Derived from Porcine Jejunum

Figure 3 provides typical and summarized results for concentration-dependent effects of NC-1059 on IPEC-J2 monolayers. Figure 3a is a trace of an IPEC-J2 monolayer exposed to 60 μM NC-1059. When exposed to 300 μM 1-EBIO, the monolayer exhibited no change in I_{sc}. Peptide exposure resulted in an increase of I_{sc} from a basal value of <1.0 to 5.5 μA cm^{-2}. I_{sc} increased to a maximal value and then declined, but not to baseline. The g_{te} increased to a peak value of 2.34 mS cm^{-2} and returned toward baseline within 30 min of peptide addition. Figure 3b provides a summary of the concentration-dependent effects of NC-1059 on maximal I_{sc} from six experiments. IPEC-J2 cells showed significant increases in maximal I_{sc} at 60 μM and greater change at 100 and 200 μM. The increase in maximal I_{sc} between 30 and 200 μM was almost linear, with a nearly threefold difference between 100 and 200 μM. The I_{sc} did not appear to reach a maximal value within the tested concentration range. Hence, equation 1 was fitted to the data with the maximal I_{sc} constrained to100 μA cm^{-2} (Table 1). IPEC-J2 cells showed a significant increase in g_{te} with 100 and 200 μM NC-1059, and the g_{te} reached a peak in 20 min or less and then began to decline toward baseline (Fig. 3c). This rapid decline in g_{te} after reaching a peak value was a common pattern observed with all concentrations of NC-1059 tested in IPEC-J2

Table 2 Parameters derived from the fit of equation 2 to g_{te} for the indicated NC-1059 concentrations[a]

Tissue	$g_{te\ max}$ (mS) 100 μM	$g_{te\ max}$ (mS) 200 μM	B (min) 100 μM	b (min) 200 μM	t_0 (min) 100 μM	t_0 (min) 200 μM
T-84	58.6 ± 5.3	58.1 ± 1.9	5.8 ± 1.2	3.8 ± 0.3	14.2 ± 1.2	8.4 ± 0.4
PVD9902	18.1 ± 1.5	51.3 ± 2.4	5.2 ± 1.1	2.4 ± 0.4	16.7 ± 1.1	6.7 ± 0.4
IPEC-J2	9.8 ± 0.4	25.2 ± 1.3	3.0 ± 0.3	1.8 ± 0.3	12.6 ± 0.3	7.7 ± 0.4
Calu-3	2.0 ± 0.7	11.0 ± 3.1	4.1 ± 1.8	4.7 ± 3.4	18.2 ± 2.0	14.2 ± 1.9

[a] Parameters refer to equation 2

monolayers. Although there was a modest decline in g_{te} in PVD9902, a pronounced decline was observed only in IPEC-J2 monolayers. The average time to reach half-maximal g_{te} (t_0), derived from the best fit with equation 2 (Table 2), was several minutes greater for 100 μM compared to 200 μM and the slope was less for 100 μM compared to 200 μM. The calculated constants from the fit (Table 2) suggest a concentration-dependent change in g_{te}. The peak change in g_{te} as a function of concentration in IPEC-J2 is shown in Fig. 3d. The change in g_{te} was nearly threefold greater at 200 μM compared to 100 μM. The difference in peak g_{te} between 100 and 200 μM was similar to the pattern observed with PVD9902 monolayers, but the peak g_{te} after exposure to NC-1059 is at least 50% lower than other epithelia for each concentration. It is also noteworthy that the graph does not reach a plateau for the concentrations tested, indicating that with higher concentration of peptide a response comparable to other epithelia may be attained.

Calu-3 Cells from Human Airway

In Fig. 4a, a Calu-3 monolayer was exposed to 300 μM 1-EBIO, and this resulted in a 30 μA cm^{-2} increase in I_{sc} that declined only modestly. Subsequent exposure to 60 μM NC-1059 increased I_{sc} by only 7 μA cm^{-2}, and there was no significant change in g_{te}. The average I_{sc} across Calu-3 monolayers after exposure to 1-EBIO and prior to addition of NC-1059 was 22 ± 5.0 μA cm^{-2}, and after exposure to 100 and 200 μM NC-1059, the average I_{sc} reached 29 ± 6.5 and 37 ± 5.5 μA cm^{-2}, respectively ($n = 6$, Fig. 4b). A fit of equation 1 to the data set was not feasible as there was a very small change in I_{sc} over the concentration range tested. Calu-3 cells showed an increase in g_{te} (Fig. 4c) after addition of NC-1059 that was relatively small compared to the change in g_{te} observed for the other epithelia that have been studied. The parameters derived from the sigmoidal fits showed small differences in t_0 for 100 and 200 μM NC-1059, and the values for slope were indistinguishable. The average peak g_{te} as a function of concentration is shown in Fig. 4d. The g_{te} at 200 μM was variable and therefore not significantly different from the g_{te} at 100 μM.

NC-1059 Allows for the Permeation of Variously Sized Dextran through Different Epithelial Monolayers

The increase in g_{te} reported above might suggest an increase in paracellular permeability. However, the electrical parameter cannot differentiate transcellular versus paracellular conductance. Hence, dextran of various sizes was used to assess permeation through the paracellular pathway. Additionally, since there were distinct differences in g_{te} before and after exposure to NC-1059, variously sized dextran was used to observe if these differences were reflected in the size selectivity to uncharged solutes.

The effects of NC-1059 on g_{te} of the various epithelia studied suggest a reduction in the paracellular barrier properties of these epithelia. MDCK monolayers treated with 100 μM NC-1059 showed an increase in permeation of 9.5 kDa, but not 77 kDa, dextran by about fivefold (Broughman et al. 2004). EDTA, an agent that disrupts epithelial monolayers, showed a much greater enhancement of permeation. In order to test the effect of NC-1059 on the paracellular route of additional cell types, the permeation of 10, 20, 40 and 70 kDa dextran was determined over a duration of 1 h across several different epithelia (Fig. 5). Permeation across monolayers exposed to 200 μM NC-1059, 5 mM EDTA or vehicle control was measured. The permeable support was freely permeable to all sizes of dextran tested (Broughman et al. 2004). NC-1059 and EDTA enhanced permeation to various sizes of dextran in all cell types tested. The epithelia differed in the amount of dextran that permeated in each case and in the pattern of permeation relative to solute size. Results specific to each cell type are presented below. Results are summarized from three experiments for each cell type.

T-84

In untreated T-84 monolayers, the permeation of dextran decreased with an increase in size. Based on Fick's law, this pattern of permeation cannot be attributed solely to diffusion rate and might be influenced by geometric constraints based on composition and length of the intercellular space, as suggested for MDCK monolayers (Spring 1998; Spring and Hope 1978). The permeation of dextran (all sizes tested) was

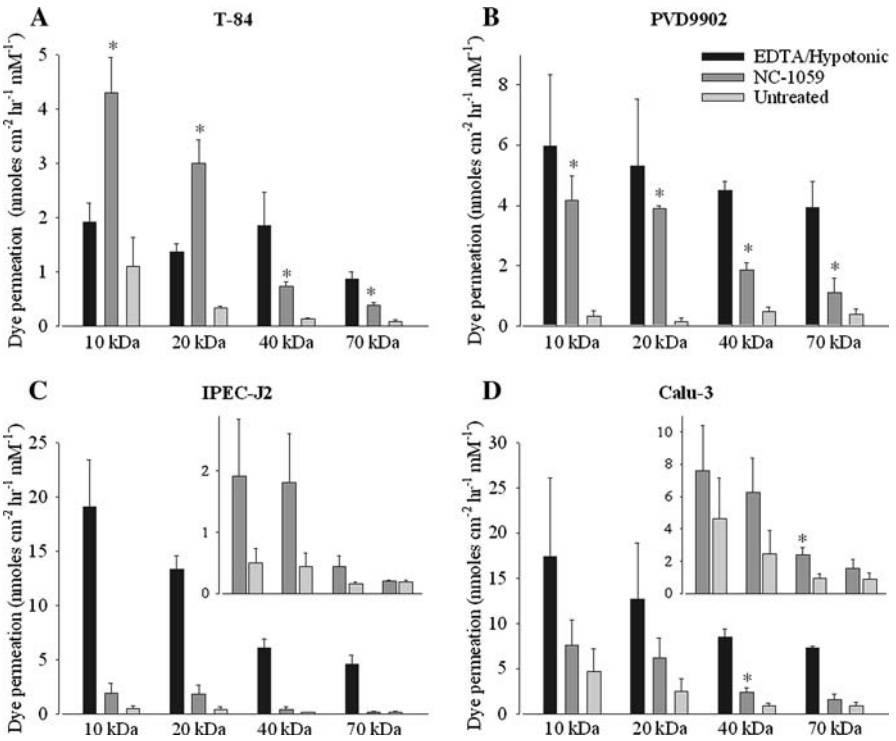

Fig. 5 NC-1059 allows for the movement of uncharged molecules across epithelial monolayers derived from a variety of mammalian sources. FITC-conjugated dextran of 10, 20, 40 and 70 kDa was added to the apical compartment; and appearance of fluorescence in the basolateral compartment was quantified in the presence of one of three treatments (EDTA solution, NC-1059 and vehicle control as described in "Methods"). In addition, dye permeation across the permeable support was quantified in the absence of cells (not shown). Dextran permeation was studied in the four different epithelia: T-84, PVD9902, IPEC-J2 and Calu-3. *Insets in the bottom panel* show dextran permeation for untreated and NC-1059-treated IPEC-J2 and Calu-3 on a different scale. (**A–D**) Data summarized from three experiments (*$P < 0.05$ for *t*-test comparing untreated vs. NC-1059-treated)

significantly greater across T-84 monolayers when treated with NC-1059 compared to untreated monolayers. The average permeation of 10 kDa dextran in the presence of NC-1059 was greater by fourfold relative to untreated monolayers and was comparable to previously published observations with MDCK monolayers (Broughman et al. 2004). Permeation of 20, 40 and 70 kDa dextran was four- to ninefold greater in NC-1059-treated monolayers than in untreated monolayers. EDTA exposure allowed for permeation of all sizes of dextran, although the relative permeation was increased less than twofold for 10 kDa dextran and about fourfold for 20 kDa dextran. There was a modest effect of EDTA on the permeation of 10 and 20 kDa dextran compared to permeation after exposure to NC-1059. However, the permeation of 40 and 70 kDa dextran was much greater in the presence of EDTA compared to NC-1059.

PVD9902

Permeation for all sizes of dextran tested in untreated PVD9902 monolayers was similar. In PVD9902 monolayers exposed to NC-1059, the average permeation of 10 kDa dextran was 12-fold greater and for 20 kDa dextran, 27-fold greater than in untreated monolayers. It should be noted that the permeation of 20 kDa across untreated monolayers was less than half that of the other dextran sizes; hence, the fold change observed was much greater. Permeation of 40 and 70 kDa dextran was fourfold and threefold greater in peptide-treated than untreated monolayers, respectively. NC-1059 induced a significant increase in permeation of all sizes of dextran. Although the permeation was enhanced for all sizes of dextran in NC-1059-treated monolayers, the absolute and relative permeation decreased with size. This suggests that there is a finite limit to the size of solute that can permeate the paracellular pathway when PVD9902 monolayers are exposed to NC-1059. Permeation for all sizes of dextran was increased to a greater extent across EDTA-treated monolayers than with NC-1059 treatment. This is consistent with EDTA-induced disruption of the tight junctions.

IPEC-J2

The permeation across untreated IPEC-J2 monolayers was comparable to PVD9902 for 10 and 20 kDa dextran and less than the rates reported for all sizes of dextran across

T-84 monolayers. NC-1059 treatment increased the permeation of dextran across IPEC-J2 monolayers of 10 and 20 kDa dextran by approximately fourfold (Fig. 5c, inset). The permeation of 40 kDa dextran was increased approximately threefold in peptide treated compared to untreated monolayers, and no NC-1059-associated difference was observed with 70 kDa dextran. Although average permeation for most sizes of dextran tested in the presence of NC-1059 was enhanced severalfold, the results did not achieve statistical significance. There was a very large increase in permeation for all sizes of dextran in the presence of EDTA, the largest of all cell types tested in both absolute and relative permeation. The results suggested that the size of the dextran molecule was the rate-limiting factor in the permeation across NC-1059-treated monolayers. The net increase in permeation for 20, 40 and 70 kDa dextran in IPEC-J2 monolayers treated with NC-1059 was relatively smaller compared to the incremental change with PVD9902 and T-84 monolayers.

Calu-3

Calu-3 cells allowed for substantially greater permeation of dextran molecules in basal conditions than the other epithelia in this study (Fig. 5d), which is consistent with the high g_{te} observed in these monolayers. Since basal permeation of all sizes of dextran is relatively high, the average permeation of all sizes of dextran tested was enhanced only approximately twofold by NC-1059 exposure. A significant increase in permeation compared to untreated monolayers was observed only in the case of 40 kDa dextran (Fig. 5d, inset). Like all other epithelia studied, EDTA enhanced permeation for all sizes of dextran by severalfold across Calu-3 cells.

Taken together the results show that NC-1059 enhances the permeation of 10–70 kDa dextran across epithelial monolayers with different tissues of origin. That g_{te} continued to increase even after I_{sc} had reached a peak value and had begun to decline suggested an increase in paracellular conductance. The dextran permeation results corroborate the conclusion that NC-1059 enhances paracellular conductance in addition to transcellular conductance. However, this simultaneous change in the transcellular and paracellular conductances across epithelial monolayers makes it difficult to isolate and quantify the changes in apical membrane conductance using an Ussing chamber. Therefore, the two-electrode voltage-clamp technique was used to study the membrane conductance induced by NC-1059, using *X. laevis* oocytes.

NC-1059 Increases Membrane Conductance in *X. laevis* Oocytes in a Dose-Dependent Manner and Remains Associated with the Oocyte Membrane for More than 2 h

The dose-dependent effect of NC-1059 on *X. laevis* oocyte membranes was determined. A typical trace showing the dose-dependent changes in oocyte membrane conductance is presented in Fig. 6a. The basal conductance was 5.81 μS. Exposure to 1.25 nmoles of NC-1059 resulted in a pronounced increase in the membrane conductance. Once the conductance reached a plateau, the addition of 2.5 nmoles NC-1059 to the flowing bath solution resulted in the membrane conductance increasing by greater than twofold when compared to 1.25 nmoles. Further addition of 5 nmoles resulted in only a small increment in conductance. The incremental change in membrane conductance with each dose was relatively small until exposure to 10 nmoles. Addition of 10 nmoles of NC-1059 increased the oocyte membrane conductance substantially to 199 μS. The addition of 20 nmoles of NC-1059, after the conductance reached a plateau, did not elicit a marked change.

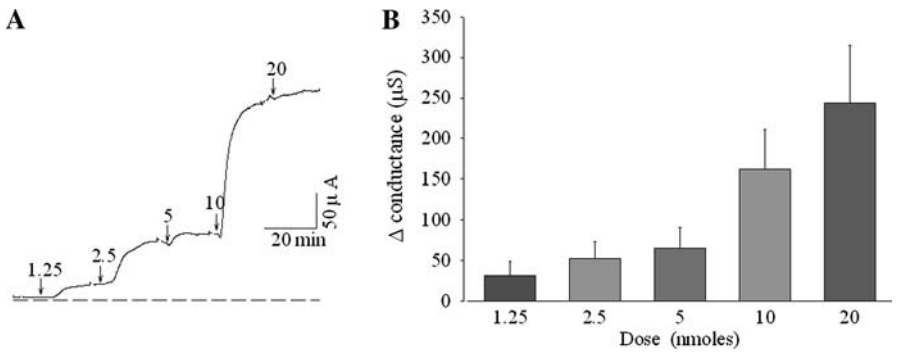

Fig. 6 (**A**) A typical trace showing that NC-1059 induces a dose-dependent change in *X. laevis* oocyte membrane conductance. *Arrows* indicate time of addition of NC-1059 to the perfusion solution. (**B**) NC-1059 induces a dose-dependent change in *X. laevis* oocyte membrane conductance. Recordings were made in a constantly perfused bath, and bolus additions of the peptide were made to the bath as indicated. Slope conductance was calculated using linear regression of current–voltage plots obtained when the current reached a plateau after each bolus addition. Each *bar* shows the average change in slope conductance from baseline (mean ± SEM for $n = 5$)

The data summarized from this experiment and four additional experiments (Fig. 6b) show an overall trend that follows the profile described for this typical trace. Slope conductance increased from 31.8 ± 17.0 μS at 1.25 nmoles to 243.5 ± 71.2 μS at 20 nmoles ($n = 5$).

NC-1059 had a dose-dependent effect on *X. laevis* oocytes similar to the observation that there was a concentration-dependent effect of NC-1059 in epithelial monolayers. Thus, a second set of experiments was conducted to observe the stability of the NC-1059-induced conductance in the oocyte membrane. A typical trace showing the effect of NC-1059 on membrane conductance is represented in Fig. 7a. Peptide (5 nmoles) was added to the perfusion solution after determining the basal conductance. The conductance increased to 150 μS, and after reaching a plateau, the conductance remained at an elevated value during the rest of the recording. Data are summarized from three experiments in Fig. 7b to show that membrane conductance increased upon exposure to NC-1059 and then remained stable during the entire recording period of 2 h. This outcome suggests that the dose-dependent change in membrane conductance induced by NC-1059 was caused by formation of ion channels in the membrane. Membrane conductance reflects the aggregate value for the number of actively gating channels (n), the single-channel conductance (g_i) and the open channel probability (P_o) of these channels ($g_{membrane} = g_i \cdot n \cdot P_o$). Although these individual properties were not determined, the aggregate value was stable over the duration of the recording.

Discussion

The results demonstrate that NC-1059, a synthetic channel-forming peptide, increased ion transport and solute permeation across epithelial monolayers derived from a variety of sources. The pattern of change in I_{sc} and g_{te} as a function of NC-1059 concentration was different in magnitude and stability for each cell type tested. Also, NC-1059-induced permeation of 10, 20, 40 and 70 kDa dextran across the various epithelia showed distinct patterns in terms of amount and size of dextran that permeated. NC-1059 increased oocyte membrane conductance in a dose-dependent manner, and the induced change in conductance remained elevated for the duration of the recording. Taken together the results suggest that NC-1059 associates with cell membranes to form stable active ion channels. The results further demonstrate that the NC-1059-induced increase in permeation across epithelial barriers, especially through the paracellular route, is not limited to MDCK monolayers and can be generated in a variety of epithelia derived from different tissues and species.

Epithelia were chosen to represent organs where efficient drug delivery is of clinical significance. The epithelia also represent a broad spectrum in terms of the degree of "tightness" (Furuse et al. 2001) as indicated by basal g_{te}. The epithelia used in the study can be arranged by degree of electrical tightness as IPEC-J2 > PVD9902 > T-84 > Calu-3 (see Table 1). The change in I_{sc} and g_{te} showed characteristically distinct patterns in the four epithelial monolayers in terms of k_{app}, Hill coefficient and time taken to reach half-maximal g_{te}, slope and the magnitude of g_{te} at different NC-1059 concentrations. The changes in I_{sc} and g_{te} observed at various peptide concentrations in T-84 monolayers are quantitatively and qualitatively similar to MDCK cells and, like MDCK cells, the k_{app} was <100 μM with T-84 cells (Broughman et al. 2004). However, in PVD9902 cell monolayers the I_{sc} did not appear to reach a maximal value within the concentration range tested. Hence, the k_{app} may be >100 μM. In the case of IPEC-J2 as well, the k_{app} may be greater than the reported value. Hill coefficients were >1 for T-84 cells and >2 for IPEC-J2 and PVD9902 cells. Both k_{app} and Hill coefficients follow this trend, IPEC-J2 > PVD9902 >T-84. Based on the constants derived from the fit of equation 2, the effect of NC-1059 on g_{te} also follows the trend IPEC-J2 > PVD9902 > T-84. Hence, it appears that the response to NC-1059 might be influenced by basal g_{te}. The lipid

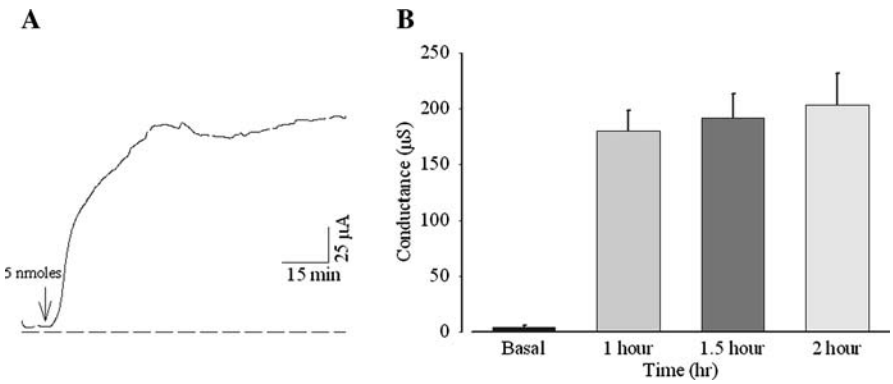

Fig. 7 (**A**) A typical trace of NC-1059-induced *X. laevis* oocyte membrane conductance as a function of time. (**B**) NC-1059 induces a stable change in *X. laevis* oocyte conductance, lasting longer than 2 h. Recordings were conducted in a constantly perfused bath. *Bars* represent average (mean ± SEM for $n = 3$) slope conductance prior to addition of peptide and after 1, 1.5 and 2 h of peptide addition

composition of membranes, particularly negatively charged lipids and cholesterol, has been shown to influence the activity of synthetic channel-forming peptides (Bell and Miller 1984; Lin and Kagan 2002), which might explain the differences in the response between epithelia.

NC-1059 increased epithelial dextran permeation, indicating that a paracellular route was accessed. In T-84 and PVD9902 monolayers, the NC-1059-induced increment in dextran permeation was greater for the smaller dextrans (10 and 20 kDa). Nevertheless, permeation for all sizes of dextran was enhanced relative to untreated monolayers. IPEC-J2 cells exhibited less permeation compared to other cell types. This is consistent with the observation that g_{te} is nearly 50% less across IPEC-J2 compared to PVD9902 and T-84 monolayers. Also, g_{te} declined rapidly in IPEC-J2 monolayers compared to a more sustained response observed in other epithelia. Since enhancing the permeability of intestinal epithelia can be associated with a risk of infection, absorption enhancers must have a transient effect. Therefore, limited and transient enhancement in permeation by NC-1059 across the IPEC-J2 monolayers is a useful property associated with the peptide in these cells derived from the small intestine. The sustained effect with T-84 cells however, demonstrates that this observation cannot be extended to all intestinal cell types. Clearly, additional studies are required to define the effects of NC-1059 on additional intestinal cell types and on native tissue.

NC-1059 produced a modest effect on ion transport across Calu-3 cell monolayers. The large and sustained effect of 1-EBIO supports the conclusion that CFTR is abundant and active in the apical membrane of unstimulated Calu-3 cells (Shen et al. 1994) and the apical conductance is not rate-limiting for ion transport. Thus, a negligible effect of NC-1059 on I_{sc} is not unexpected. Nonetheless, 100 and 200 μM NC-1059 increased g_{te}, which we interpret as an increase in paracellular permeability. Ultimately, the amount of dextran that permeated Calu-3 monolayers in the presence of NC-1059 was comparable to that observed in the other epithelia studied. The ability of NC-1059 to enhance permeation by 10 to 20 kDa molecules across Calu-3 monolayers suggests that it might be used to enhance delivery of drugs in nasal sprays or inhalers.

NC-1059 increased paracellular passage of dextrans up to 70 kDa, although permeation was quite low. Larger molecules were not tested in this study. Earlier work in MDCK cells, however, showed no passage of 2.5 MDa dextran (Broughman et al. 2004). Taken together, the results suggest that permeation of small molecules (e.g., vancomycin) will be enhanced by NC-1059. Permeation of larger molecules such as insulin ($\sim$4 kDa) will also likely be enhanced by NC-1059, but molecules such as albumin (67 kDa) would be expected to have limited permeability. Permeability of larger and potentially harmful structures, such as bacteria and virus particles, would also be expected to remain negligible.

Epithelial cells differ in size, and hence, the monolayers may differ in the number of lateral intercellular spaces. Additionally, epithelia may differ in the composition, distribution and expression of the junctional proteins that maintain the integrity of the paracellular route (Acharya et al. 2004; Heiskala, Peterson and Yang 2001). Both of these factors can contribute to the differences observed in the epithelia studied. Tight junctions are "multimolecular complexes" comprised of integral membrane proteins and plaque proteins. These plaque proteins are associated with several cytosolic proteins and connect the integral membrane proteins and perijunctional actin cytoskeleton (Schneeberger and Lynch 2004). These proteins have an integral role in regulating paracellular permeability (Anderson and Van Itallie 1995; Furuse et al. 1996; McCarthy et al. 1996). Disruption of actin and the localization of junctional proteins by toxins such as ZOT (Fasano 2000) reportedly resulted in increased paracellular permeability. Our present results show that NC-1059 enhances permeation through the paracellular space. The results suggest that, in addition to supporting ion transport across epithelial cells, NC-1059 transiently affects the stability or distribution of tight junction proteins.

NC-1059 induces a rapid and dose-dependent increase in membrane conductance in *X. laevis* oocytes. It is noteworthy that the membrane conductance consistently changed in small increments until the 5 nmole dose and addition of 10 nmoles caused a more substantial change in conductance. Exposure to a higher dose inconsistently caused a modest change in membrnae conductance that did not achieve statistical significance. A possible explanation is that 10 nmoles establishes a critical concentration in the membrane at which individual peptide molecules are sufficiently close to assemble into the greatest number of functional channels and possibly to saturate the membrane such that further peptide exposure does not enhance conductance.

NC-1059 induced an increase in membrane conductance that remained stable in *Xenopus* oocytes as opposed to the transient effect on I_{sc} observed in mammalian epithelial monolayers. This suggests that there is a secondary event in the epithelial monolayers responsible for the decrease in I_{sc} (i.e., results suggest that channel-forming peptides can remain resident in the cell membrane). One possibility is that NC-1059 forms channels that cause depolarization. The decrease in I_{sc} may occur when cellular mechanisms are not sufficient to maintain electrochemical driving forces to sustain net ion transport at the peak level. Long, stable recordings with both mammalian cell monolayers and *Xenopus* oocytes, however, demonstrate that the peptide does not induce cell lysis.

The predominant obstacle to the permeation of clinically relevant therapeutics across epithelial barriers is the degree of hydrophilicity and size for many of these molecules. Systemic drug delivery for such compounds requires larger doses of drugs and therefore is associated with increased costs and the potential for undesirable effects in some cases (Torchilin 2000). Several oral antibiotics and antivirals have limited permeability across intestinal epithelia because of their hydrophilic nature and size (Peppas et al. 2004). Colonic, airway and corneal/conjuctival epithelia are barriers to the absorption of drugs specifically targeted to these tissues. Conditions that afflict the anterior portion of the eye, such as glaucoma and keratitis, are treated with drugs that must permeate the corneal or conjuctival epithelia (Edward and Prausnitz 2001; Zhang et al. 2004). The nasal or airway epithelium is another major target for drug delivery as an alternative to injections of drugs such as insulin (Gonzalez et al. 2006; Turker et al. 2004). Results presented here show that NC-1059 enhanced the permeation of molecules as large as 10 and 20 kDa across colonic (T-84), small intestinal (IPEC-J2) and airway (Calu-3) epithelial monolayers. NC-1059 also enhanced permeation across kidney (MDCK) (Broughman et al. 2004) and reproductive duct (PVD9902) epithelial monolayers. Hence, NC-1059 has the potential to be developed as an absorption enhancer for therapeutic agents.

Acknowledgements We thank Gary Radke and Ryan Carlin for their technical assistance. This article is contribution 08-76-J from the Kansas Agriculture Experiment Station. This study was supported in part by Public Health Service grants GM 066620 and GM 074096 (both to J. M. T.).

References

Acharya P, Beckel J, Ruiz WG, Wang E, Rojas R, Birder L, Apodaca G (2004) Distribution of the tight junction proteins ZO-1, occludin, and claudin-4, -8, and -12 in bladder epithelium. Am J Physiol 287:F305–F318

Anderson JM, Van Itallie CM (1995) Tight junctions and the molecular basis for regulation of paracellular permeability. Am J Physiol 269:G467–G475

Bell JE, Miller C (1984) Effects of phospholipid surface charge on ion conduction in the K^+ channel of sarcoplasmic reticulum. Biophys J 45:279–287

Broughman JR, Mitchell KE, Sedlacek RL, Iwamoto T, Tomich JM, Schultz BD (2001) NH_2-terminal modification of a channel-forming peptide increases capacity for epithelial anion secretion. Am J Physiol 280:C451–C458

Broughman JR, Shank LP, Prakash O, Schultz BD, Iwamoto T, Tomich JM, Mitchell K (2002a) Structural implications of placing cationic residues at either the NH2- or COOH-terminus in a pore-forming synthetic peptide. J Membr Biol 190:93–103

Broughman JR, Shank LP, Takeguchi W, Schultz BD, Iwamoto T, Mitchell KE, Tomich JM (2002b) Distinct structural elements that direct solution aggregation and membrane assembly in the channel-forming peptide M2GlyR. Biochemistry 41:7350–7358

Broughman JR, Brandt RM, Hastings C, Iwamoto T, Tomich JM, Schultz BD (2004) Channel-forming peptide modulates transepithelial electrical conductance and solute permeability. Am J Physiol 286:C1312–C1323

Carlin RW, Sedlacek RL, Quesnell RR, Pierucci-Alves F, Grieger DM, Schultz BD (2006) PVD9902, a porcine vas deferens epithelial cell line that exhibits neurotransmitter-stimulated anion secretion and expresses numerous HCO_3^- transporters. Am J Physiol 290:C1560–C1571

Chung NP, Mruk D, Mo MY, Lee WM, Cheng CY (2001) A 22–amino acid synthetic peptide corresponding to the second extracellular loop of rat occludin perturbs the blood–testis barrier and disrupts spermatogenesis reversibly in vivo. Biol Reprod 65:1340–1351

Devor DC, Singh AK, Bridges RJ, Frizzell RA (1996a) Modulation of Cl^- secretion by benzimidazolones. II Coordinate regulation of apical G_{Cl} and basolateral G_K. Am J Physiol 271:L785–L795

Devor DC, Singh AK, Frizzell RA, Bridges RJ (1996b) Modulation of Cl^- secretion by benzimidazolones. I Direct activation of a Ca^{2+}-dependent K^+ channel. Am J Physiol 271:L775–L784

Edward A, Prausnitz MR (2001) Predicted permeability of the cornea to topical drugs. Pharm Res 18:1497–1508

Everett RS, Vanhook MK, Barozzi N, Toth I, Johnson LG (2006) Specific modulation of airway epithelial tight junctions by apical application of an occludin peptide. Mol Pharmacol 69:492–500

Fasano A (2000) Regulation of intercellular tight junctions by zonula occludens toxin and its eukaryotic analogue zonulin. Ann N Y Acad Sci 915:214–222

Fasano A, Fiorentini C, Donelli G, Uzzau S, Kaper JB, Margaretten K, Ding X, Guandalini S, Comstock L, Goldblum SE (1995) Zonula occludens toxin modulates tight junctions through protein kinase C-dependent actin reorganization, in vitro. J Clin Invest 96:710–720

Fasano A, Uzzau S (1997) Modulation of intestinal tight junctions by zonula occludens toxin permits enteral administration of insulin and other macromolecules in an animal model. J Clin Invest 99:1158–1164

Furuse M, Fujimoto K, Sato N, Hirase T, Tsukita S (1996) Overexpression of occludin, a tight junction-associated integral membrane protein, induces the formation of intracellular multilamellar bodies bearing tight junction-like structures. J Cell Sci 109(Pt 2):429–435

Furuse M, Furuse K, Sasaki H, Tsukita S (2001) Conversion of zonulae occludentes from tight to leaky strand type by introducing claudin-2 into Madin-Darby canine kidney I cells. J Cell Biol 153:263–272

Gonzalez C, Kanevsky D, De Marco R, Di Girolamo G, Santoro S (2006) Non-invasive routes for insulin administration: current state and perspectives. Expert Opin Drug Deliv 3:763–770

Heiskala M, Peterson PA, Yang Y (2001) The roles of claudin superfamily proteins in paracellular transport. Traffic 2:93–98

Kondoh M, Yagi K (2007) Progress in absorption enhancers based on tight junction. Expert Opin Drug Deliv 4:275–286

Lacaz-Vieira F, Jaeger MM, Farshori P, Kachar B (1999) Small synthetic peptides homologous to segments of the first external loop of occludin impair tight junction resealing. J Membr Biol 168:289–297

Lin MC, Kagan BL (2002) Electrophysiologic properties of channels induced by Abeta25–35 in planar lipid bilayers. Peptides 23:1215–1228

McCarthy KM, Skare IB, Stankewich MC, Furuse M, Tsukita S, Rogers RA, Lynch RD, Schneeberger EE (1996) Occludin is a functional component of the tight junction. J Cell Sci 109(Pt 9):2287–2298

Peppas NA, Wood KM, Blanchette JO (2004) Hydrogels for oral delivery of therapeutic proteins. Expert Opin Biol Ther 4:881–887

Schneeberger EE, Lynch RD (2004) The tight junction: a multifunctional complex. Am J Physiol 286:C1213–C1228

Shen BQ, Finkbeiner WE, Wine JJ, Mrsny RJ, Widdicombe JH (1994) Calu-3: a human airway epithelial cell line that shows cAMP-dependent Cl^- secretion. Am J Physiol 266:L493–L501

Spring KR (1998) Routes and mechanism of fluid transport by epithelia. Annu Rev Physiol 60:105–119

Spring KR, Hope A (1978) Size and shape of the lateral intercellular spaces in a living epithelium. Science 200:54–58

Tavelin S, Hashimoto K, Malkinson J, Lazorova L, Toth I, Artursson P (2003) A new principle for tight junction modulation based on occludin peptides. Mol Pharmacol 64:1530–1540

Thompson SE, Cavitt J, Audus KL (1994) Leucine enkephalin effects on paracellular and transcellular permeation pathways across brain microvessel endothelial cell monolayers. J Cardiovasc Pharmacol 24:818–825

Tomich JM, Wallace D, Henderson K, Mitchell KE, Radke G, Brandt R, Ambler CA, Scott AJ, Grantham J, Sullivan L, Iwamoto T (1998) Aqueous solubilization of transmembrane peptide sequences with retention of membrane insertion and function. Biophys J 74:256–267

Torchilin VP (2000) Drug targeting. Eur J Pharm Sci 11(Suppl 2):S81–S91

Turker S, Onur E, Ozer Y (2004) Nasal route and drug delivery systems. Pharm World Sci 26:137–142

Wallace DP, Tomich JM, Iwamoto T, Henderson K, Grantham JJ, Sullivan LP (1997) A synthetic peptide derived from glycine-gated Cl^- channel induces transepithelial Cl^- and fluid secretion. Am J Physiol 272:C1672–C1679

Wong V, Gumbiner BM (1997) A synthetic peptide corresponding to the extracellular domain of occludin perturbs the tight junction permeability barrier. J Cell Biol 136:399–409

Zhang W, Prausnitz MR, Edwards A (2004) Model of transient drug diffusion across cornea. J Control Release 99:241–258